

# Parametric Blur Estimation for Blind Restoration of Natural Images: Linear Motion and Out-of-Focus

João P. Oliveira, *Member, IEEE*, Mário A. T. Figueiredo, *Fellow, IEEE*,  
and José M. Bioucas-Dias, *Member, IEEE*

**Abstract**—This paper presents a new method to estimate the parameters of two types of blurs, linear uniform motion (approximated by a line characterized by angle and length) and out-of-focus (modeled as a uniform disk characterized by its radius), for blind restoration of natural images. The method is based on the spectrum of the blurred images and is supported on a weak assumption, which is valid for the most natural images: the power-spectrum is approximately isotropic and has a power-law decay with the spatial frequency. We introduce two modifications to the Radon transform, which allow the identification of the blur spectrum pattern of the two types of blurs above mentioned. The blur parameters are identified by fitting an appropriate function that accounts separately for the natural image spectrum and the blur frequency response. The accuracy of the proposed method is validated by simulations, and the effectiveness of the proposed method is assessed by testing the algorithm on real natural blurred images and comparing it with state-of-the-art blind deconvolution methods.

**Index Terms**—Image restoration, linear motion and out-of-focus blur, natural images, parametric blur estimation.

## I. INTRODUCTION

IN IMAGE deconvolution/deblurring, the goal is to estimate an original image  $f$  from an observed image  $g$ , assumed to have been produced according to

$$g = f * h + n, \quad (1)$$

where  $h$  is the blur *point spread function* (PSF),  $n$  is a set of independent samples of zero-mean Gaussian noise of variance  $\sigma^2$ , and  $*$  denotes the two-dimensional (2D) convolution. In standard deconvolution, it is assumed that  $h$  is known. In *blind image deconvolution* (BID), one seeks an estimate of the image  $f$ , under (total or partial) lack of knowledge about the blurring operator  $h$  [6], [20], [21]. BID is clearly harder than its non-blind counterpart; the problem becomes ill-posed both with respect to the unknown image and the blur operator. Simply put (and because convolution corresponds to a product in the

Manuscript received August 8, 2012; revised March 15, 2013 and June 10, 2013; accepted September 26, 2013. Date of publication October 18, 2013; date of current version December 12, 2013. This work was supported by Fundação para a Ciência e Tecnologia under Grants PTDC/EEA-TEL/104515/2008, Pest-OE/EEI/LA0008/2011, and PTDC/EEI-PRO/1470/2012. The associate editor coordinating the review of this manuscript and approving it for publication was Dr. Farhan A. Baqai.

J. P. Oliveira is with the Instituto de Telecomunicações, Instituto Superior Técnico, Lisboa 1049-001, Portugal, and also with the Instituto Universitário de Lisboa (ISCTE-IUL), Lisboa 1649-026, Portugal (e-mail: joao.oliveira@lx.it.pt).

M. A. T. Figueiredo and J. M. Bioucas-Dias are with the Instituto de Telecomunicações, Instituto Superior Técnico, Lisboa 1049-001, Portugal (e-mail: mario.figueiredo@lx.it.pt; jose.bioucas@lx.it.pt).

Color versions of one or more of the figures in this paper are available online at <http://ieeexplore.ieee.org>.

Digital Object Identifier 10.1109/TIP.2013.2286328

Fourier domain), BID can be seen as the problem of recovering two functions from their product; a clearly hopeless goal, in the absence of strong assumptions or prior knowledge about the underlying image and blur. Assumptions about the blur PSF have included positiveness, known shape (*e.g.*, Gaussian blur), smoothness, symmetry, or known finite support [6].

There are two main alternative approaches to BID: **(i)** simultaneously estimate the image and the blur [1], [2], [9]; **(ii)** obtain a blur estimate from the observed image and then use it in a non-blind deblurring algorithm [7], [24]. Most of the proposed methods are of type **(i)**; in practice, many of those methods follow the strategy of alternating between estimating the blur kernel and the image. To do so, prior knowledge about the image and the blur are usually formalized, under a Bayesian or a regularization framework. What distinguishes the different methods is the objective function to be optimized, which results from the priors/regularizers adopted to model the original image and the blur PSF [6].

In this paper, we propose a blur estimation technique to be used in an approach of type **(ii)**. More specifically, we extend our previous work [33] and introduce a method to estimate the parameters of a linear uniform (constant velocity) motion blur or an out-of-focus blur, from the noisy blurred image, under weak assumptions on the underlying original image. All the methods proposed in the literature assume some form of prior knowledge about the image. This is usually expressed by modeling the statistics of some feature(s), such as first order differences, the Laplacian, or some other local operators characterized by sparse representations (*e.g.* wavelets, curvelets, DCT). These methods usually depend on several parameters that need to be obtained a priori, either from similar images, or manually adjusted.

The method herein proposed does not involve any critical parameter, thus it is, in this sense, truly blind for the class of blur filters considered. The only assumptions are that the original image is natural (meaning that it has an approximately isotropic power spectrum) and that the blur results from either linear uniform motion or wrong focusing.

This paper is organized as follows. Section II starts by reviewing state-of-the-art and related work. Section III-A presents the natural image model, formalizes the linear uniform motion and out-of-focus blur models and their parameters, and the blurred image spectral model. In Section IV, we introduce a modified Radon transform, which plays a central role in the proposed method presented in Section V. Finally, Section VI reports experimental results, both on synthetic examples and real blurred natural color images, including

comparisons with state-of-the-art methods, namely those of Fergus *et al* [11], Xu and Jia [47], and Amit *et al* [13].

## II. RELATED WORK AND CONTRIBUTIONS

This section reviews previous BID methods, with emphasis on those that are closest to the approach proposed in this paper.

Fergus *et al* [11] introduced a BID method that uses natural image statistics to estimate the blur kernel; they use ensemble learning [27], based on a prior on the derivative of the underlying image, and a variational method to approximate the posterior. Levin [23] uses the same prior as Fergus *et al* [11], but follows a different approach by searching for the kernel that brings the distribution of the deblurred image closest to the observed distribution. The blur direction is then estimated as that of minimal derivative variation and subsequently the blur length is selected by choosing the best fit using  $k$ -tap blurs. Although the method can in principle work in any direction, the only results presented are for short horizontal motion blurs.

Shan *et al* [41] proposed a unified probabilistic framework that iterates between blur kernel estimation and latent image recovery. To avoid ringing artifacts, the authors use a model of the spatially random noise distribution and a smoothness constraint on the latent image, in areas of low contrast. The effect of these constraints also propagates to the kernel refinement stage. Xu and Jia [47] proposed a two-phase kernel estimation algorithm, based on a spatial prior to select salient edges, which yields good initial kernel estimates; subsequently, a kernel refinement stage is carried out, using an iterative support detection algorithm [46]. The method avoids hard thresholding of the kernel elements, often used by other methods to impose sparsity, and achieves state-of-the-art results. In very recent work, Xu *et al* [48] proposed an  $\ell_0$ -based image regularizer for motion deblurring.

Goldstein *et al* [13] proposed a new method for recovering the blur kernel, based on statistical irregularities of the power spectrum. Depending on the image nature, large and strong edges introduce a bias term in the typical power law of natural images. The method introduces a new model and a spectral whitening formula to estimate the power spectrum of the blur. The blur PSF is then recovered using a phase retrieval algorithm. In the approach followed by Jia [17], the blur PSF is recovered from the transparency of blurred object boundaries. Edges were also exploited by Joshi *et al* [18], who start by detecting blurred edges and predict the underlying sharp ones, under the strong assumption that they were originally step edges; those authors claim that if the image has edges spanning all the directions, the blurred and predicted sharp image contain enough information to estimate the blur PSF.

Some approaches try to reduce the ill-posed nature of BID; *e.g.*, Rav-Acha *et al* [37] use information of two motion-blurred images, while Yuan *et al* [49] use a pair of images (one blurred, one noisy). Other methods aim at reducing the ill-posedness by using specialized hardware [26], [31], [36].

Some blurs are identifiable without resorting to priors or regularizers, namely if their frequency response has a known parametric form that can be characterized by its frequency domain zeros. Two of these are the linear uniform motion

blur and the out-of-focus blur [8]. Linear uniform motion blur (a special case of motion blur) is a reasonable model for small motions (*e.g.*, a hand-held camera with a moderate exposure time) and a very accurate model in the context of digital aerial imaging [25], [12], [22]. For example, the system described in [22] uses different apertures for the RGB channels, leading to different exposure times; the resulting image thus suffers from linear uniform motion blur, with different values on different channels. The other case herein considered, out-of-focus blur, is one of the most common blur types, which occurs when the camera is not properly focused, thus the focal plane is away from the sensor plane [3].

The *Fourier transform* (FT) of the blurs mentioned in the previous paragraph are sinc-like and Bessel-like functions, respectively [3], with the distance between consecutive zeros depending directly on the blur length. The so-called zero-crossing methods rely on identifying these patterns in the frequency domain; this is often a difficult task, due to noise, which may degrade the performance of these methods. In order to circumvent this weakness, some authors have exploited the non-stationary nature of the images versus the stationarity of the blur; this is the case of the *power cepstral* method [4], [35], which exploits the FT of the logarithm of the power spectrum. In the cepstral domain, a large spike will occur wherever there is a periodic pattern of zeros in the original Fourier domain. The location of this spike can be used to infer the parameters of the linear motion blur. An extension of this idea led to the power bispectrum [10], which is more robust to noise.

Recently, the *Radon transform* (RT) [5] of the spectrum of the blurred image has been proposed for motion blur estimation [19], [28]. The idea is that along the direction perpendicular to the motion, the zero pattern will correspond to local minima. The motion angle can thus be estimated as the one for which the maximum of the Radon transform occurs [28], or that for which the entropy is maximal [19]. The motion blur length is then estimated using fuzzy sets in [28], and cepstral features, in [19]. Instead of working directly on the spectrum of the blurred image, the method in [16] exploits the same ideas on the image gradients. Other methods exploiting the existence of zero patterns in the Fourier domain include the Hough transform employed in [39] and the correlation of the spectrum with a detecting function [44].

Out-of-focus blurs have received comparably less attention, and are usually addressed using general BID methods. Sun *et al* [43] used particle swarm optimization and wavelet transforms, while Moghaddam *et al* [29] proposed using the Hough transform of the spectrum; that method requires high SNR ( $>55$ dB) to be successful.

In this paper, we propose new methods to estimate the parameters of linear uniform motion blurs (characterized by the length and direction) and out-of-focus blurs (characterized by the radius). We improve upon our previous work [33] in several ways. We introduce a new parametric model, combined with two modified Radon transforms, which includes two terms: one that approximates the image spectrum and another one approximating the blur spectrum (a sinc-like function, in the motion blur case, and a Bessel function in the out-of-focus case). For the linear motion blur case, we propose

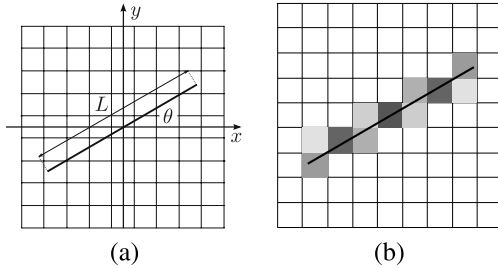


Fig. 1. Proposed discretized kernel for linear motion blur. (a) Bright spot of light traveling across discrete sensor grid, length  $L$  and angle  $\theta$ . (b) Resulting kernel—gray shades are proportional to the length of the intersection of the line segment with each pixel.

to change the integration limits of the Radon transform, and show that this change improves the angle and length estimation accuracy: the quasi-isotropic power spectrum of natural images allow using the same parametric model independently of the motion angle. For out-of-focus blurs, the zero patterns of the corresponding Bessel functions in the Fourier domain are circular; to capture this behavior, we use a circular Radon transform, which, as far as we know, had not been used before in the context of blur estimation. These new features allow accurately estimating longer blurs with sub-pixel precision.

Although our method is parametric, it has several advantages. Firstly, it relies on a weak assumption, which is valid for most natural images: the power-spectrum is approximately isotropic and has a power-law decay with respect to spatial frequency. Secondly, it is faster than statistical methods, as it does not use any iterations, and scales well with the image size (the most expensive operation is a single global FFT). Finally, experimental results show that the proposed method is competitive with state-of-the-art BID methods.

### III. BLUR MODELS AND SPECTRA

In this section, we introduce the statistical model of natural images that underlies the proposed approach, and formally describe the two types of blurs considered.

#### A. Natural Image Model

A relevant characteristic of natural images [7], [14], [45] concerns its spectral behaviour. Let  $F(\xi, \eta)$  denote the 2D FT of an image  $f(x, y)$ . Consider the family of lines  $\eta = \xi \tan \varrho$  (in the  $(\xi, \eta)$  plane) passing through the origin at angle  $\varrho$ . Along these lines, the power spectrum falls off with  $|\xi|$ , roughly independently of  $\varrho$ ; a standard model for this behavior is

$$\log |F(\xi, \xi \tan \varrho)| \simeq a |\xi|^b, \quad (2)$$

where  $a > 0$  [7]. As pointed out in [13], spectral irregularities may occur, due to strong edges. These irregularities may depend on  $\varrho$ , making  $a$  also dependent on  $\varrho$ . In the proposed method, however, this effect will be attenuated, as the different lines of the spectra will be integrated, as explained in Section IV.

#### B. Linear Uniform Motion Blur

Linear uniform motion blur results from the linear movement of the entire image, along one direction. We assume that

these movements are due to camera translation with no in-plane rotation nor changes of focus. We also assume that the whole scene is far away from the camera, thus the whole image is equally affected by the motion, yielding a spatially invariant blur<sup>1</sup>. This kind of blur occurs in digital aerial imaging, where the camera travels along a line parallel to the scene (the ground). It also occurs in small camera movements, when the length of the blur kernel is small enough.

In a continuous domain [9], a linear uniform motion blur PSF is a normalized delta function, supported on a line segment with length  $L$  at an angle  $\theta$  (e.g., with respect to the horizontal; see Fig. 1 (a)) [3]. The angle  $\theta$  depends on the motion direction, and the length  $L$  is proportional to the motion speed and duration of exposure. This model corresponds to considering a bright spot moving along a straight line segment centered at the origin.

A discrete version is obtained by considering this bright spot [9] moving over the image pixels; as this point traverses the different sensors with constant velocity, and assuming that each sensor is linear and cumulative, the response is proportional to the time spent over that sensor. Thus, we obtain the corresponding intensity of each pixel of the blur kernel by computing the length of the intersection of the line segment with each pixel in the grid (see Fig. 1 (b)). To preserve the energy, the kernel is then normalized.

#### C. Out-of-Focus Blur

Out-of-focus blurring occurs if the camera is not properly focused, thus the focal plane is away from the sensor plane. In this case, a single bright spot spreads among its neighboring pixels, yielding a uniform disk [3]. The more unfocused the image is, the larger the radius of this disk. Different depths maps yield disks with different sizes; thus, we assume that the focal distance is at infinity. This assumption works reasonably well for the majority of natural images where the scene is far away from the camera. Savakis *et al* [40] showed that a more accurate (and complex) model of out-of-focus blur does not improve the restoration quality, comparing with this simple model. In the continuous case [9], the resulting out-of-focus blur PSF is thus a normalized disk [3]:

$$h(x, y) = \begin{cases} \frac{1}{\pi R^2}, & \text{if } \sqrt{x^2 + y^2} \leq R \\ 0, & \text{otherwise.} \end{cases} \quad (3)$$

In the discrete domain, each PSF value will be proportional to the intersection area between the continuous blur and the corresponding pixel. Again, to preserve the energy, the kernel is normalized. Note that, in this case, a blur is characterized by only one parameter: its radius  $R$ .

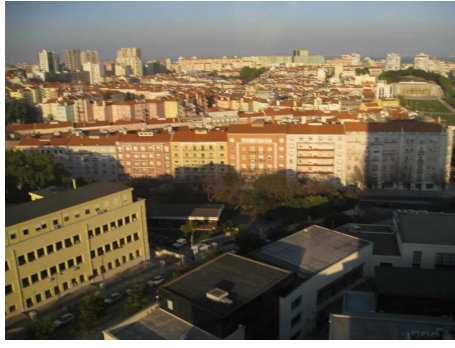
#### D. Blurred Image Spectra

Taking the Fourier transform of (1) leads to

$$G(\xi, \eta) = F(\xi, \eta) H(\xi, \eta) + N(\xi, \eta), \quad (4)$$

where  $F, G, H$ , and  $N$  are the Fourier transforms of  $f, g, h$ , and  $n$ , respectively. As usual in deconvolution problems, we

<sup>1</sup>The spatially invariant blur allows writing the convolution with an invariant kernel, much smaller than the image.



(a)



(b)

Fig. 2. (a) Natural color image (size  $3264 \times 2448$ ) with linear motion blur. (b) Natural color image (size  $5184 \times 3456$ ) with out-of-focus blur (both acquired with a Canon Ixus 850).

assume that the noise is weak, supporting the approximation

$$\begin{aligned} \log |G(\xi, \eta)| &\approx \log |F(\xi, \eta)| H(\xi, \eta)| \\ &= \log |F(\xi, \eta)| + \log |H(\xi, \eta)|; \end{aligned} \quad (5)$$

*i.e.*, the coarse behavior of  $\log |G(\xi, \eta)|$  depends essentially on  $\log |F(\xi, \eta)| + \log |H(\xi, \eta)|$ . Since the coarse behavior  $\log |F(\xi, \eta)|$  along lines  $\eta = \xi \tan \varrho$  in the  $(\xi, \eta)$  plane is approximately independent of  $\varrho$  (see (5)), the structure of  $\log |H(\xi, \eta)|$ , namely its zeros, is preserved in  $\log |G(\xi, \eta)|$ . However, the presence of noise may prevent these “zeros” from being exact. Nevertheless, they remain close to zero, and more importantly, they are local minima.

Since linear uniform motion blur is modeled by a line segment, the corresponding spectrum is a sinc-like function in the direction of the blur. In this case, the spectrum exhibits zeros along lines perpendicular to the motion direction, separated from each other by a distance that depends on the blur length. Fig. 3 (a) shows the logarithm of the power spectrum of the natural image shown in Fig. 2 (a), which suffered linear uniform motion blur. Namely due to the presence of noise and other model mismatches, the zeros become local minima; nevertheless, one can easily recognize the motion blur pattern. To identify the motion angle, we propose to use a modified Radon transform (RT) described in detail in Section IV. The idea is to integrate the spectrum of the blurred image along different directions; the integration performed perpendicularly to the angle of the motion blur will best exhibit the sinc-like behavior, namely because the log power spectrum of the underlying natural image is (approximately) angle-independent. This is illustrated in Fig. 3 (b).

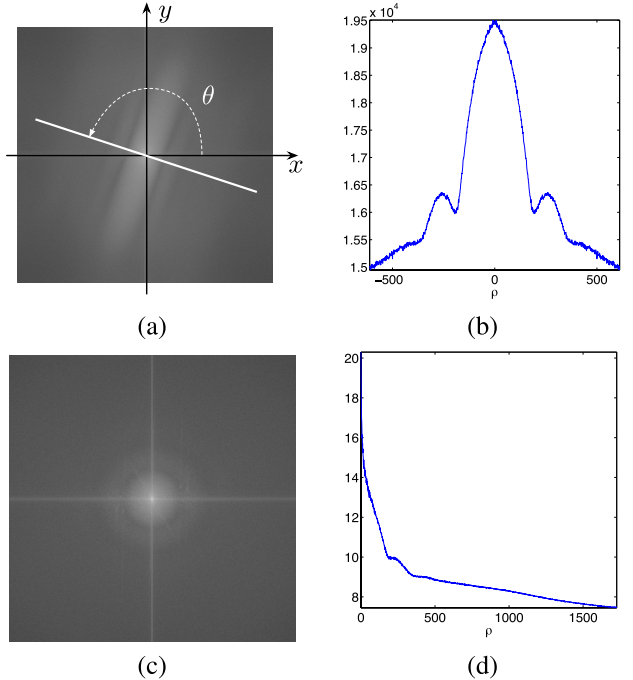


Fig. 3. Image of Fig. 2-(a): (a) logarithm of the power spectrum (white line segment indicates motion direction), (b) Radon transform of spectrum at the motion blur angle ( $\theta = 155^\circ$ ). Image of Fig. 2-(b): (c) logarithm of the power spectrum (magnified), (d) Radon-c transform of spectrum.

The out-of-focus blur, on the other hand, is modeled by an uniform disk, and has a Bessel-like spectrum [42]. In this case, the local minima are along circles, the radii of which depend on the PSF radius. To capture these circular zero patterns (or local minima), we propose a Radon-type transform (termed Radon-c) that integrates along circles, rather than straight lines, as describe in Section IV. Fig. 2 (b) shows a natural color image corrupted by out-of-focus blur; in Fig. 3 (c) and (d) we can observe the circular pattern, both in the power spectrum of the image and on the circular Radon transform.

#### IV. MODIFIED RADON TRANSFORMS

The Radon transform (RT) is an integral transform that consists of the integral of a function along straight lines [5]. Formally, the RT of a real-valued function  $\phi(x, y)$  defined on  $\mathbb{R}^2$ , at angle  $\theta$ , and distance  $\rho$  from the origin, is given by

$$\mathcal{R}(\phi, \rho, \theta) = \int_{-\infty}^{\infty} \int_{-\infty}^{\infty} \phi(x, y) \delta(\rho - x \cos \theta - y \sin \theta) dx dy,$$

where  $\delta$  denotes the Dirac delta function. Equivalently,

$$\mathcal{R}(\phi, \rho, \theta) = \int_{-\infty}^{\infty} \phi(\rho \cos \theta - s \sin \theta, \rho \sin \theta + s \cos \theta) ds.$$

The RT  $\mathcal{R}(\phi, \rho, \theta)$  is the integral of  $\phi$  along a line forming an angle  $\theta$  with the  $x$ -axis, at a distance  $\rho$  from the origin [5]. The Radon transform is used in many scientific and technical fields, in particular in computed tomography [15], [30].

In this paper, we introduce two modifications to the RT. As noted above, natural images have an approximate coarse behavior of  $\log |G(\xi, \eta)|$  along lines that pass through the origin, independently of the angle. We capture this behavior in two different ways: **(i)** performing the Radon Transform with

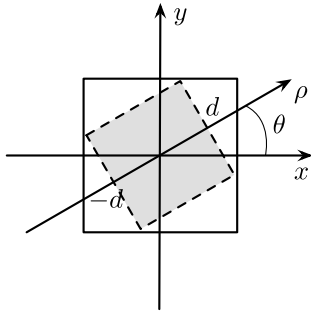


Fig. 4. Illustration of Radon-d integration limits: the gray square represents the maximum inscribed square.

the same integration area for different angles; (ii) integrating along circles, rather than parallel straight lines.

#### A. Radon-d Transform

The Radon-d modification of the RT performs integration over the same area, independently of the direction of integration. This is achieved by, instead of computing the RT of the whole image, changing the integration limits to contain only the maximum inscribed square, as illustrated in Fig. 4, *i.e.*,

$$\mathcal{R}_d(f, \rho, \theta) = \begin{cases} \int_{-d}^d f(\rho \cos \theta - s \sin \theta, \rho \sin \theta + s \cos \theta) ds, & |\rho| \leq d \\ 0, & \text{otherwise,} \end{cases} \quad (6)$$

with  $d = m/\sqrt{2}$  (where  $m = \min\{N, M\}$ , for an  $N \times M$  image). This modified RT (called Radon-d) of  $\log |G(\xi, \eta)|$  has approximately the same energy, independently of  $\theta$ .

Consider the natural image represented in Fig. 5. The corresponding Radon-d transform of the logarithm of the magnitude of its Fourier transform is depicted in Fig. 6-(a), for different angles. As shown in [32], this Radon-d transform of a natural image can be approximated by a line, as a consequence of the fact that the spectrum follows the power law mentioned in Section III-A. However, the spectral irregularities pointed out in [13], as well as the two lines that can be observed at  $0^\circ$  and  $90^\circ$  (due to the use of the FFT [34]), make the integration not exactly a line.

Thus, to better approximate the Radon-d transform of a natural image, we propose fitting a third order polynomial,

$$\mathcal{R}_d(\log |F|, \rho, \theta) \approx a \rho^3 + b \rho^2 + c \rho + d. \quad (7)$$

In Fig. 6-(b) we plot a line of the Radon-d transform of the logarithm of the spectrum magnitude of the natural image in Fig. 5, and the approximation given by Equation (7).

#### B. Radon-c Transform

Limiting the integration interval is not the only way to capture the quasi-invariant angular behavior of  $\log |G(\xi, \eta)|$ . Instead, we may integrate along circles with radius  $\rho$ , *i.e.*, perform integration directly in polar coordinates,

$$\mathcal{R}_c(f, \rho) = \frac{1}{2\pi\rho} \int_{-\pi}^{\pi} f(\rho \cos \theta, \rho \sin \theta) d\theta, \quad (8)$$

which we call *Radon-c*. Notice that if  $f$  equals 1 (in the 2-D plane),  $\mathcal{R}_c$  will be equal to 1, independently of  $\rho$ , due to the normalization factor  $1/(2\pi\rho)$ .



Fig. 5. Image of size  $3264 \times 2448$  (acquired with a Canon Ixus 850).

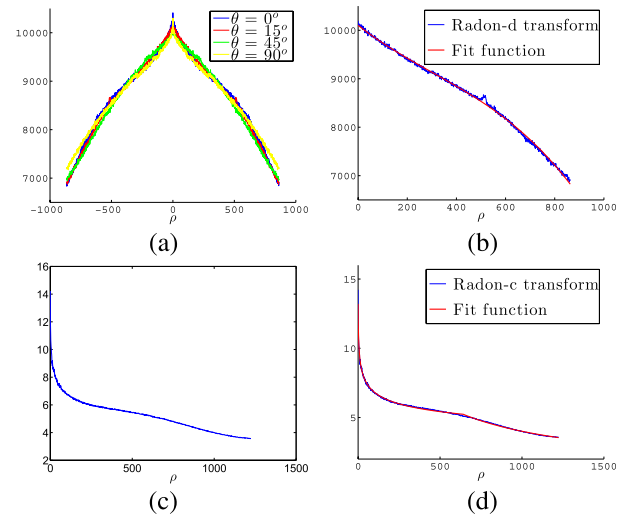


Fig. 6. (a) Radon-d transform of the logarithm of the spectral magnitude of the image in Fig. 5 ( $\rho$  in pixel units). (b) Fitted function (7). (c) Radon-c transform of Fig. 5. (d) Fitted function (9).

In Fig. 6(c), we plot the Radon-c transform of the logarithm of the spectrum magnitude of the natural image in Fig. 5. Since the integration is along circles, the Radon-c transform is closely related with the approximation given by Equation (5). After an exhaustive experimental study, the Radon-c transform of natural images is very similar to the one depicted in Fig. 6(c). To better approximate it, specially in the higher frequencies, we propose a two-region power law function,

$$\mathcal{R}_c(\log |F|, \rho) \simeq \begin{cases} a |\rho|^b, & \rho \leq \rho_0 \\ d |\rho|^c + e, & \rho > \rho_0 \end{cases} \quad (9)$$

where  $d = \frac{ab}{c} \rho_0^{b-c}$  and  $e = a \rho_0^b - d \rho_0^c$ , since the approximate function must be continuous at  $\rho = \rho_0$ . Fig. 6-(d) shows the Radon-c transform, together with the approximate model (9), for the natural image of Fig. 5.

## V. PROPOSED ALGORITHM

We now introduce the proposed algorithms to infer the parameters of linear uniform motion blurs and out-of-focus blurs. For the linear uniform motion case, the parameters to

estimate are the angle and the length. In the out-of-focus case, the only parameter is the radius.

Once we have computed one of the modified RTs mentioned in the previous section, the blur parameter (*i.e.*, the motion length or the disk radius) estimation will be performed by fitting an appropriate function to the result. According to (5), and the linearity of the RT, the proposed function has two terms: one for the image spectrum, and the other one for the blur frequency response  $H$ , *i.e.*, omitting the dependency on  $\theta$ ,

$$\gamma(\rho) = \underbrace{\mathcal{R}_d(\log|F|, \rho, \theta)}_{\gamma_F(\rho)} + \underbrace{\mathcal{R}_d(\log|H|, \rho, \theta)}_{\gamma_H(\rho)}. \quad (10)$$

The previous equation refers to the linear uniform motion blur case; for the out-of-focus blur, we simply replace  $\mathcal{R}_d$  with  $\mathcal{R}_c$ .

The image spectrum term  $\gamma_F(\rho)$  is approximated by (7) or (9), accordingly. The blur spectrum term is approximated by

$$\gamma_H(\rho) \simeq \alpha \log(1 + \beta \log|H(\rho)|), \quad (11)$$

where  $|H(\rho)|$  is defined in the following subsections, and parameters  $\alpha$  and  $\beta$  are introduced to take into account the non linearities and the noise. Since noise prevents the “zeros” of the blur spectra from being exact, this can only be achieved by the term  $1 + \beta$  inside the logarithm. Parameter  $\alpha$  controls the relative weight of the blur spectral term against the image spectra. This term is proportional to the integration limits of the RT, because the magnitude of the blur spectrum is constant in the integration direction, *i.e.*, along straight lines for linear uniform motion blur, and circular lines for out-of-focus blur. These parameters are needed since (5) is just an approximation.

### A. Motion Blur

The sinc-like structure of the motion blur kernel [3] is well captured by the Radon-d transform at the blur angle. Thus, motion blur estimation will be done in two phases: **(i)** angle estimation; **(ii)** motion length estimation.

In [28], the angle estimate is that for which the maximum of the RT occurs; naturally, this only works for very long blurs, so that the blurred image is very smooth in the motion blur direction, leading to a clear maximum of the RT. On the other hand, in [19], the angle estimate is the one for which  $\mathcal{R}(\phi, \rho, \theta)$ , as a function of  $\rho$ , has the highest entropy.

The spectral irregularities and the artifacts introduced by the FFT make it difficult for the previous approaches to work well for short blurs. To increase the robustness and take advantage of the quasi-invariance of the spectra, [32] computes the difference of the RT at perpendicular angles and chooses the one that has the maximum energy. In this paper, we follow a simpler approach, where the main goal is to identify the blur pattern in the Radon-d transform. Computing the Radon-d transform of the linear motion blur spectrum, we obtain a sinc structure in the blur direction, and a constant line in the perpendicular direction. Thus, by fitting the model in Equation (7) to the Radon-d transform, which integrates the quasi-invariance of the image spectra plus the blur spectra, the fitting error will be maximum precisely at the motion

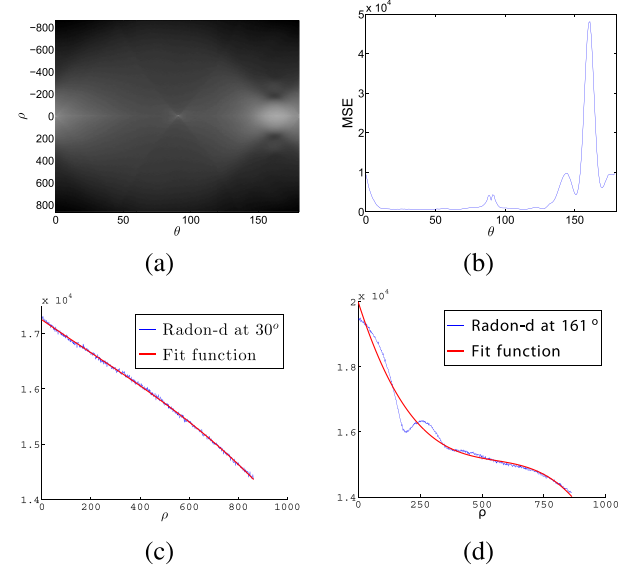


Fig. 7. Illustration of the motion blur angle estimation criterion. (a)  $\mathcal{R}_G(\rho, \theta)$  as a function of  $\rho$  and  $\theta$ , represented by gray levels. (b) Residual  $\sum_p (\mathcal{R}_G(\rho, \theta) - \hat{\mathcal{R}}_G(\rho, \theta))^2$  as a function of  $\theta$ . (c)  $\mathcal{R}_G(\rho, \theta)$  and  $\hat{\mathcal{R}}_G(\rho, \theta)$ , as a function of  $\rho$  (in pixel units), for  $\theta = 30^\circ$ . (d)  $\mathcal{R}_G(\rho, \theta)$  and  $\hat{\mathcal{R}}_G(\rho, \theta)$ , for  $\theta = 161^\circ$  (the correct angle).

angle<sup>2</sup>. Let  $\mathcal{R}_G(\rho, \theta)$  denote the integral of  $\log|G(\xi, \eta)|$  along a direction perpendicular to  $\theta$ , *i.e.*,

$$\mathcal{R}_G(\rho, \theta) = \mathcal{R}_d(\log|G(\xi, \eta)|, \rho, \theta). \quad (12)$$

Consider also the function  $\hat{\mathcal{R}}_G(\rho, \theta)$  given by fitting an approximation of the form (7) to  $\mathcal{R}_G(\rho, \theta)$ . The proposed angle estimate is that which maximizes the mean squared error (MSE) of this fit,

$$\hat{\theta} = \arg \max_{\theta} \sum_{\rho} (\mathcal{R}_G(\rho, \theta) - \hat{\mathcal{R}}_G(\rho, \theta))^2. \quad (13)$$

In Fig. 7, several plots illustrate the angle estimation criterion given by (13), applied to the image of Fig. 2(a).

Once we have  $\hat{\theta}$ , we proceed to estimate the length of the blur kernel. Given that the sinc-like behavior is preserved in the Radon transform at angle  $\hat{\theta}$ , we base the blur length estimation on  $\mathcal{R}_{\hat{\theta}}$ . We proceed by fitting  $\gamma(\rho)$  (see (10)) to  $\mathcal{R}_G(\rho, \hat{\theta})$ . In this case,  $\gamma_F(\rho)$  is given by (7), and  $H(\omega)$  must be proportional to a sinc function [3], *i.e.*,

$$|H(\omega)| \propto |\text{sinc}(\lambda\omega)|, \quad (14)$$

where  $\text{sinc}(x) = \frac{\sin(\pi x)}{\pi x}$ , and  $\lambda$  is the blur length.

The joint estimate of all the parameters *i.e.*,  $\{a, b, c, d, \lambda, \alpha, \beta\}$ , may not yield the right solution, as the corresponding least squares criterion is highly non-convex, thus any iterative minimization algorithm is doomed to be trapped at local minima. Instead, we first minimize with respect to  $\{a, b, c, d, \alpha, \beta\}$ , with  $\lambda$  fixed, thus obtaining a function of  $\lambda$  alone, which is then minimized by line search. The previously estimated parameters  $\{a, b, c, d\}$  are used, in a refinement stage, as initial values to fit Equation (7)

<sup>2</sup>The integration of the blur spectrum, perpendicularly to the motion direction, yields a constant value, well approximated by Eq. (7).

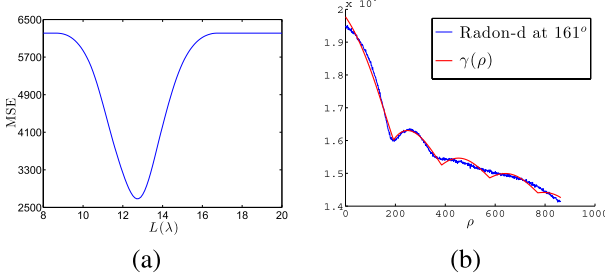


Fig. 8. RT and corresponding approximate function. (a) MSE of fitted function  $\gamma(\rho)$  as a function of  $L$ . (b)  $R_G(\rho, \hat{\theta})$  and adjusted function  $\gamma(\rho)$ .

to the data, with  $\{\alpha, \beta\}$  initialized with positive values (typically  $\approx 1$ ). Parameter  $\lambda$  is chosen to be the value leading to the minimum mean squared error. In Fig. 8, we show the Radon-d transform at  $\hat{\theta}$ , the root mean squared error as a function of  $\lambda$ , and the approximated function (10) for the motion blurred image of Fig. 2 (a).

The normalized discrete Fourier angular frequency  $\omega$  is related to the continuous frequency  $\Omega$  by  $\omega = \Omega T$  [34]; since we have  $N$  different angular frequencies ( $N$  is the number of points), each real frequency is given by:

$$\Omega_k = \frac{2\pi k}{NT}, \quad k = 0, \dots, N-1. \quad (15)$$

Assuming that the image is square with size  $N \times N$ , from (15), we finally have  $\widehat{L} = \frac{\lambda}{N}$ .

### B. Out-of-Focus Blur

To infer the radius of the out-of-focus blur, we proceed as in the motion blur case. However, since the pattern of zeros in the spectrum is now circular, we use the *Radon-c* transform and do not have any angle to estimate. The fitting function is again the one in (10), where  $\gamma_F(\rho)$  is given by (9), and

$$|H(\omega)| \propto \left| \frac{J_1(\lambda \omega)}{\lambda \omega} \right|, \quad (16)$$

where  $J_\delta$  is the Bessel function of the first kind, with parameter  $\delta$  [42]. The set of parameters to estimate is  $\{a, b, c, \xi_0, \lambda, \alpha, \beta\}$ . Again, since the criterium is highly non-convex, we proceed as in the previous case: we fix  $\lambda$  and optimize for the rest of the parameters; we initialize  $\{a, b, c, \xi_0\}$  by the values that fit (9) alone, and assign a small positive number to  $\{\alpha, \beta\}$ ; we pick  $\lambda$  that leads to the minimum mean squared error. Like in the previous case, from (16) we have  $\widehat{R} = \frac{2\pi \lambda}{N}$ . In Fig. 9, we show the Radon-d transform at  $\hat{\theta}$ , the root mean squared error as a function of  $\lambda$ , and the approximated function (10) for the motion blurred image of Fig. 2 (b).

## VI. EXPERIMENTAL RESULTS

We assess the performance of the proposed method in two different ways. First, we use synthetically blurred images, exactly given by the models described in Section III. The accuracy is assessed by the root mean squared error (RMSE) of the estimated parameters:

$$\text{RMSE} = \sqrt{\frac{1}{n} \sum_i (x - \hat{x}_i)^2},$$

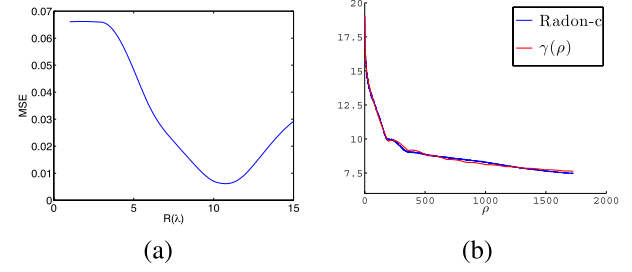


Fig. 9. RT and corresponding approximate function. (a) MSE of fitted function  $\gamma(\rho)$  as a function of  $R$ . (b)  $R_G(g, \rho)$  and adjusted function  $\gamma(\rho)$ .

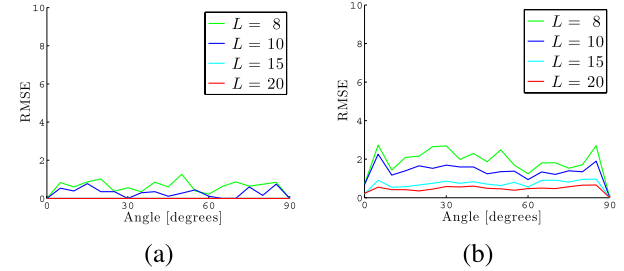


Fig. 10. RMSE (in degrees) of the angle estimation algorithm, for two noise scenarios. (a) BSNR = 40dB. (b) BSNR = 20dB (where BSNR denotes ‘blurred SNR’, given by  $\equiv 10 \log_{10}(\text{var}[blurred\ image]/\sigma^2)$ , and  $\sigma$  is the noise variance, as defined in Section I).

where  $n$  is the number of runs,  $x$  and  $\hat{x}_i$  are the true parameter and its estimate in the  $i$ -th run, respectively. Finally, we apply the method to real BID problems; in this case, the linear motion blur and out-of-focus assumptions are only approximations. In the real BID experiments, we compare the proposed method with several state-of-the-art alternatives.

### A. Accuracy of Proposed Algorithm

The accuracy of the proposed method is assessed in terms of RMSE over  $n = 10$  runs (in degrees for the angular parameter, and pixel units for length parameters). To this end, we considerer a set of 7 well-known images: cameraman, Lena, Barbara, boats, peppers, goldhill ( $256 \times 256$ ), fingerprint ( $512 \times 512$ ), and also the natural image of Fig. 5.

Fig. 10 shows the accuracy of the proposed method: the errors are similar and essentially independent of the true angle. The highest errors are obtained for the smallest lengths, which is a natural result; in fact, for a very short motion blur, the kernels obtained with two close angles are almost identical. The accuracy of the algorithm also depends on the natural image assumption (namely its spectral isotropy): if an image is not a natural image, the quasi-invariance of the image spectrum does not hold, making the angle identification more difficult.

Concerning length estimation, the errors are also quite small, even for large blur lengths (Fig. 11). This is a major improvement over our previous algorithm [33], for which one of the weaknesses was precisely for long blurs. By using the fitting function  $\gamma(\rho)$  (10), the method is no longer dependent on the location of the first local minimum, and can also achieve sub-pixel precision. This is important in the case of natural motion blurred images, where the length of the blur can result

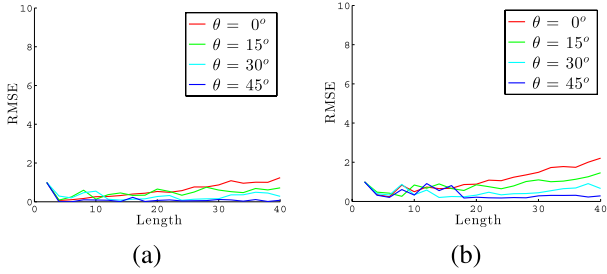


Fig. 11. RMSE (in pixel units) of the length estimation algorithm, for two noise scenarios. (a) BSNR = 40dB. (b) BSNR = 20dB.



Fig. 14. Natural images corrupted with (approximately linear) motion blur, acquired with a Canon Ixus 850.

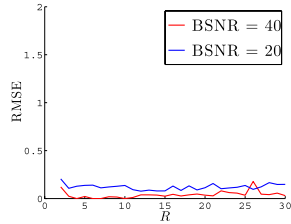


Fig. 12. RMSE (in pixel units) of the out-of-focus blur estimation algorithm, for two noise scenarios.

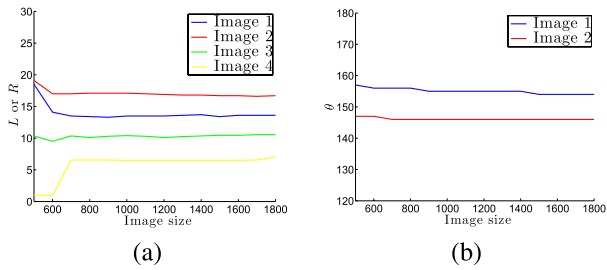


Fig. 13. Estimated parameters as a function of image size. (a) and (b) Images 1 and 2 are those in Fig. 14, Images 3 and 4 are those in Fig. 18.

in equivalent blur lengths with sub-pixel precision, depending on the sampling rate.

Fig. 12 shows the accuracy of the proposed algorithm for the out-of-focus case. These results show that the algorithm is accurate and, as expected, the errors are relatively larger for smaller blurs. For small blurs, the first zero (local minimum) of the blur spectrum corresponds to larger values of  $\rho$ , which is approximated by the second term in (9). Nevertheless, the algorithm correctly copes with these cases.

Finally, Fig. 13 shows the estimated blur angle and length obtained from the natural blurred images, as a function of image size. We consider square crops of the images depicted in Fig. 14 and Fig. 18. As expected, the performance of the algorithm decreases with the image size, but it only degrades considerably for image sizes below  $600 \times 600$  pixels, which is totally acceptable.

### B. Natural Blurred Images

We consider now a set of images obtained with a common hand-held camera, corrupted with (approximately linear) motion blur and out-of-focus blur. Due to the large size of the images, deblurring was done with the Richardson-Lucy algorithm [38], separately for each color channel. Since we



Fig. 15. Closeups of the blurred images from Fig. 2-(a) (top) and from Fig. 14 (bottom).

don't have ground truth, only a qualitative visual comparison can be made. We compare our results with three state-of-the-art BID methods, for which there is code available: **(i)** the method proposed by Fergus *et al* [11]; **(ii)** the method of Goldstein *et al* [13], which is related to our method; **(iii)** the method of Xu *et al* [47], considered state-of-the-art when compared against others methods (we are thus indirectly also comparing our method with all the methods considered in [47]). Full size images and more examples can be seen at <http://preview.tinyurl.com/ce96nsb>.

*1) Motion Blur:* To simulate motion blur (not "camera shake"), we performed an out of plane rotation of a far away scene. This way, all the elements of the image move approximately the same, making valid the space invariant blur approximation. Note that this is an approximation, and that some in plane rotation may be present. In Figs. 2-(a) and 14, we show natural linear motion blurred images. A graphical representation of the blur estimates obtained, as well as closeups showing the corrupted images and corresponding restorations are depicted in Figs. 15, 16 and 17.

The image estimates produced by our approach are visually quite good. Comparing with the results of the other methods, we can observe that some details are recovered better. Notice, in particular, some details for which we know a priori their original shape, such as the "P" sign in Fig. 16 or a circular lamp in Fig. 17. We can see in all the examples (and also on those available at <http://preview.tinyurl.com/ce96nsb>) that the different methods produce kernel estimates with similar lengths and directions. However, unlike the others, our method imposes the continuity of the kernel.

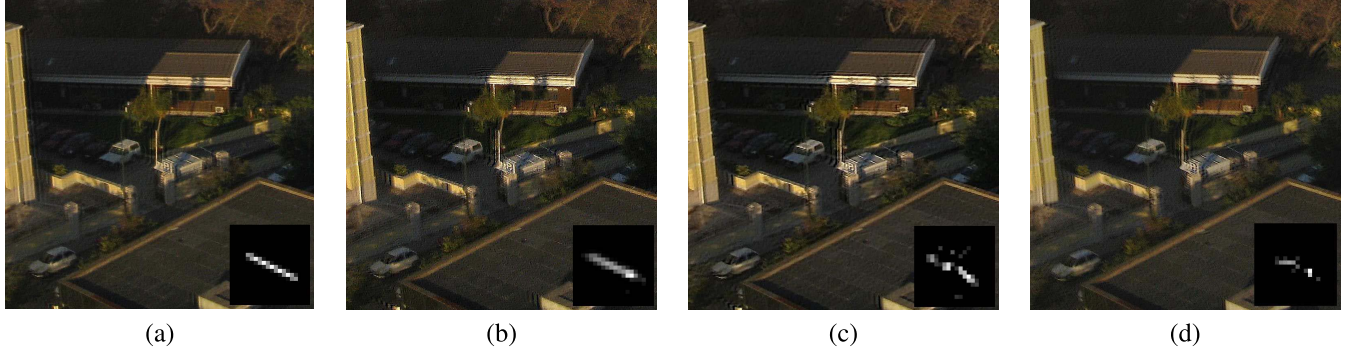


Fig. 16. Closeups of the restored images and estimated kernels. (a) Proposed method. (b) Method of Xu *et al* [47]. (c) Method of Goldstein *et al* [13]. (d) Method of Fergus *et al* [11].

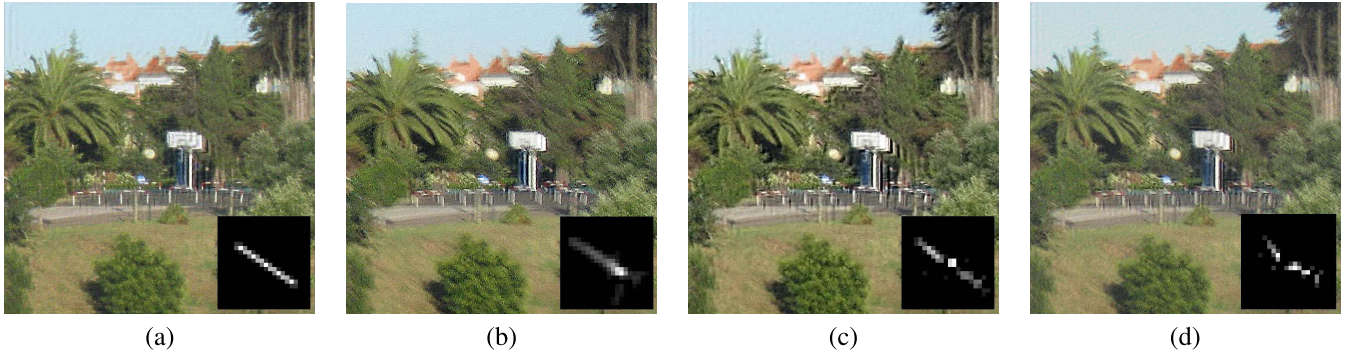


Fig. 17. Closeups of restored images and estimated kernels. (a) Proposed method. (b) Method of Xu *et al* [47]. (c) Method of Goldstein *et al* [13]. (d) Method of Fergus *et al* [11].

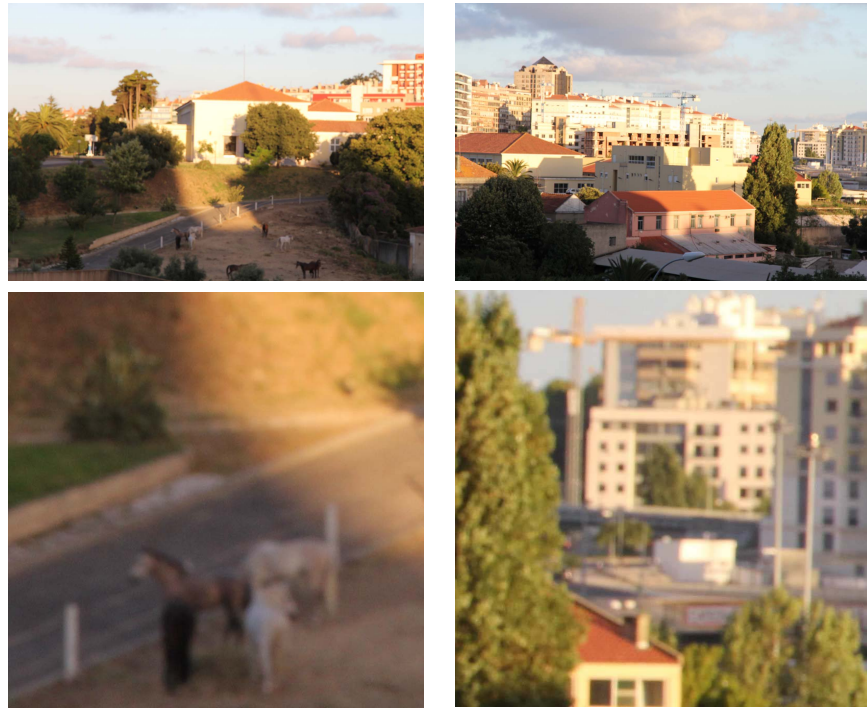


Fig. 18. Natural images corrupted with out-of-focus blur (acquired with a Canon D60) and closeups thereof.

A MATLAB implementation of our algorithm (running on 2.2GHz Core 2 Duo) took around 10 minutes to restore the natural color images shown in this section. The method

proposed in [11] takes around 1 hour. It was not possible to restore the full size images with methods and code proposed in [47] and [13], due to its huge dimensions. Considering

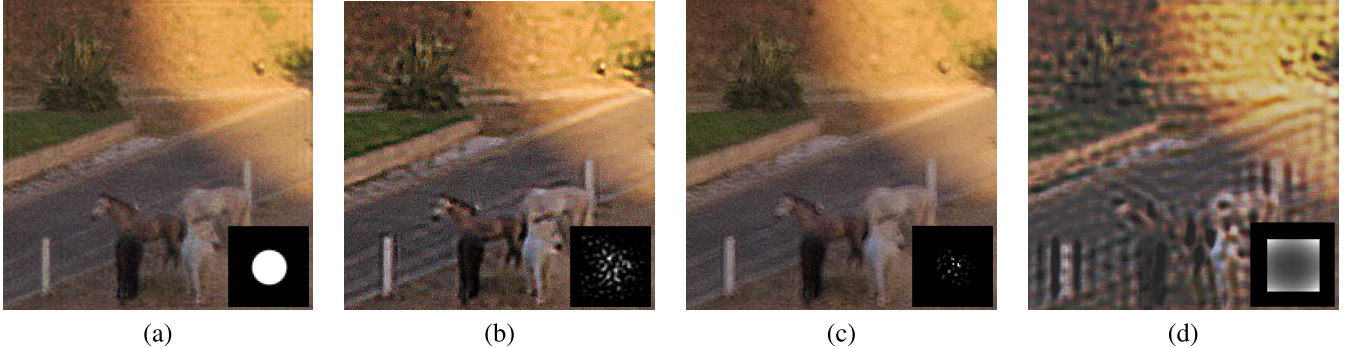


Fig. 19. Closeups of restored images and estimated kernels. (a) Proposed method. (b) Xu *et al* [47]. (c) Goldstein *et al* [13]. (d) Fergus *et al* [11].

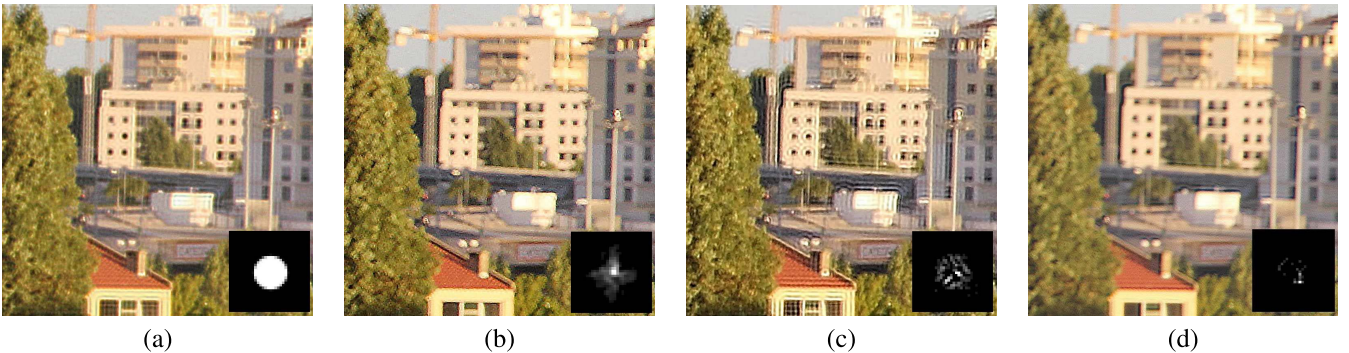


Fig. 20. Closeups of restored images and estimated kernels. (a) Proposed method. (b) Xu *et al* [47]. (c) Goldstein *et al* [13]. (d) Fergus *et al* [11].

only the close up versions (800 by 800 pixels), our method took around 33 seconds, Xu *et al* [47] 58 seconds, and Goldstein *et al* [13] 92 seconds.

2) *Out-of-Focus*: The images used in these experiments were taken on a tripod, to ensure that the images are free from motion blur. The scenes are far away from the camera, making the focal distance at infinity assumption valid. Fig. 18 shows the original blurred images. The estimated kernels as well the closeups of the restored images are depicted in Figs. 19 and 20. As can be seen, the restored images with our method are visually good. The estimated kernels are, different in shape, but consistent in the support size. Once again, our better results comes from the fact that the proposed kernel is compact and close to the true one. In terms of speed, the restoration times were similar to the linear motion blur case.

## VII. CONCLUSION

We have proposed a new method to estimate the parameters for two standard classes of blurs: linear uniform motion blur and out-of-focus. These classes of blurs are characterized by having well defined patterns of zeros in the spectral domain. The method proposed in this paper works on the spectrum of the blurred images, and is supported on the weak assumption that the underlying images satisfy the following natural image property: the power-spectrum is approximately isotropic and has a power-law decay with respect to the distance to the origin of the spatial frequency plane

To identify the patterns of linear motion blur and out-of-focus blur, we introduced two modifications to the Radon transform, termed *Radon-d* and *Radon-c*. The former is

characterized by performing integration over the same area of the image spectrum, while the later performs integration along circles. The identification of the blur parameters is made by fitting appropriate functions that account separately for the natural image spectrum and the blur spectrum.

The accuracy of the proposed method was validated by simulations, and its effectiveness was assessed by testing the algorithm on real blurred natural images. The restored images were also compared with those produced by state-of-the-art methods for blind image deconvolution.

## REFERENCES

- [1] M. Almeida and L. Almeida, "Blind and semi-blind deblurring of natural images," *IEEE Trans. Image Process.*, vol. 19, no. 1, pp. 36–52, Jan. 2010.
- [2] L. Bar, N. Sochen, and N. Kiryati, "Variational pairing of image segmentation and blind restoration," in *Proc. 8th ECCV*, 2004, pp. 166–177.
- [3] M. Bertero and P. Boccacci, *Introduction to Inverse Problems in Imaging*. England, U.K.: IOP Publishing, 1998.
- [4] B. P. Bogert, M. J. R. Healy, and J. W. Tukey, "The quefrency analysis of time series for echoes: Cepstrum, Pseudo Autocovariance, Cross-Cepstrum and saphe cracking," in *Proc. Symp. Time Ser. Anal.*, vol. 15, 1963, pp. 209–243.
- [5] R. Bracewell, *Two-Dimensional Imaging*. Upper Saddle River, NJ, USA: Prentice-Hall, 1995.
- [6] P. Campisi and K. Egiazarian, *Blind Image Deconvolution: Theory and Applications*. Cleveland, OH, USA: CRC Press, 2007.
- [7] A. S. Carasso, "Direct blind deconvolution," *SIAM J. Appl. Math.*, vol. 61, no. 6, pp. 1980–2007, 2001.
- [8] T. F. Chan and J. Shen, *Image Processing and Analysis - Variational, PDE, Wavelet, Stochastic Methods*. Philadelphia, PA, USA: SIAM, 2005.
- [9] T. F. Chan and C. K. Wong, "Total variation blind deconvolution," *IEEE Trans. Image Process.*, vol. 7, no. 3, pp. 370–375, Mar. 1998.

- [10] M. Chang, A. Tekalp, and A. Erdem, "Blur identification using the bispectrum," *IEEE Trans. Signal Process.*, vol. 39, no. 10, pp. 2323–2325, Oct. 1991.

[11] R. Fergus, B. Singh, A. Hertzmann, S. T. Roweis, and W. Freeman, "Removing camera shake from a single photograph," *ACM Trans. Graph. SIGGRAPH*, vol. 25, pp. 787–794, Aug. 2006.

[12] K. Gao, X.-X. Li, Y. Zhang, and Y.-H. Liu, "Motion-blur parameter estimation of remote sensing image based on quantum neural network," in *Proc. Int. Conf. Opt. Instrum. Tecnol., Optoelectron. Imag. Process. Technol.*, 2011, pp. 82001L-1–82001L-11.

[13] A. Goldstein and R. Fattal, "Blur-kernel estimation from spectral irregularities," in *Proc. ECCV*, 2012, pp. 622–635.

[14] A. Hyvärinen, J. Hurri, and P. O. Hoyer, *Natural Image Statistics: A Probabilistic Approach to Early Computational Vision*, 2nd ed. New York, NY, USA: Springer-Verlag, 2009.

[15] A. Jain, *Fundamentals of Digital Image Processing*. Upper Saddle River, NJ, USA: Prentice-Hall, 1989.

[16] H. Ji and C. Liu, "Motion blur identification from image gradients," in *Proc. IEEE Conf. CVPR*, Jun. 2008, pp. 1–8.

[17] J. Jia, "Single image motion deblurring using transparency," in *Proc. IEEE Conf. CVPR*, Jun. 2007, pp. 1–8.

[18] N. Joshi, R. Szeliski, and D. J. Kriegman, "PSF estimation using sharp edge prediction," in *Proc. IEEE Conf. CVPR*, Jun. 2008, pp. 1–8.

[19] F. Krahmer, Y. Lin, B. McAdoo, K. Ott, J. Wang, D. Widemann, et al., "Blind image deconvolution: Motion blur estimation," *Inst. Math. Appl.*, Univ. Minnesota, Minneapolis, Minnesota, Tech. Rep. 2133-5, 2006.

[20] D. Kundur and D. Hatzinakos, "Blind image deconvolution," *IEEE Signal Process. Mag.*, vol. 13, no. 3, pp. 43–64, May 1996.

[21] D. Kundur and D. Hatzinakos, "Blind image deconvolution revisited," *IEEE Signal Process. Mag.*, vol. 13, no. 6, pp. 61–63, Nov. 1996.

[22] L. Lelégard, E. Delaygue, M. Brédif, and B. Vallet, "Detecting and correcting motion blur from images shot with channel-dependent exposure time," in *Proc. Annal. ISPRS*, vols. 1–3. 2012, pp. 341–346.

[23] A. Levin, "Blind motion deblurring using image statistics," in *Proc. Adv. NIPS*, 2006, pp. 841–848.

[24] A. Levin, Y. Weiss, F. Durand, and W. Freeman, "Efficient marginal likelihood optimization in blind deconvolution," in *Proc. IEEE Conf. CVPR*, Jun. 2011, pp. 2657–2664.

[25] M. Liu, G. Liu, J. Xiu, H. Kuang, and L. Zhai, "Aerial image blurring caused by image motion and its restoration using wavelet transform," *Proc. SPIE*, vol. 5637, pp. 425–433, Feb. 2005.

[26] X. Liu and A. Gamal, "Simultaneous image formation and motion blur restoration via multiple capture," in *Proc. IEEE ICASSP*, vol. 3, May 2001, pp. 1841–1844.

[27] J. Miskin and D. Mackay, "Ensemble learning for blind image separation and deconvolution," in *Proc. Adv. Independ. Compon. Anal.*, 2000, pp. 123–141.

[28] M. Moghaddam and M. Jamzad, "Motion blur identification in noisy motion blur identification in noisy images using fuzzy sets," in *Proc. 5th IEEE Int. Symp. Signal Process. Inf. Technol.*, Dec. 2005, pp. 862–866.

[29] M. Moghaddam, "A mathematical model to estimate out of focus blur," in *Proc. ISPA 5th Int. Symp.*, Sep. 2007, pp. 278–281.

[30] F. Natterer, *The Mathematics of Computerized Tomography*. New York, NY, USA: Wiley, 1986.

[31] S. K. Nayar and M. B. Ezra, "Motion-based motion deblurring," *IEEE Trans. Pattern Anal. Mach. Intell.*, vol. 26, no. 6, pp. 689–698, Jun. 2004.

[32] J. P. Oliveira, "Advances in total variation image restoration: Blur estimation, parameter estimation and efficient optimization," Ph.D. dissertation, Inst. Superior Técnico, Univ. Montana, Missoula, MT, USA, Jul. 2010.

[33] J. P. Oliveira, M. A. T. Figueiredo, and J. M. Bioucas-Dias, "Blind estimation of motion blur parameters for image deconvolution," in *Proc. 3rd Iberian Conf. IbPRIA*, 2007, pp. 604–611.

[34] A. Oppenheim and R. Schafer, *Discrete-Time Signal Processing*, 2nd ed. Upper Saddle River, NJ, USA: Prentice-Hall, 1999.

[35] J. G. Proakis and D. G. Manolakis, *Digital Signal Processing*. Upper Saddle River, NJ, USA: Prentice-Hall, 2007.

[36] R. Raskar, A. Agrawal, and J. Tumblin, "Coded exposure photography," *ACM Trans. Graph. SIGGRAPH*, vol. 3, no. 25, pp. 95–804, 2006.

[37] A. Rav-Acha and S. Peleg, "Two motion blurred images are better than one," *Patter Recognit. Lett.*, vol. 25, pp. 311–317, Feb. 2005.

[38] W. H. Richardson, "Bayesian-based iterative method of image restoration," *J. Opt. Soc. Amer.*, vol. 62, no. 1, pp. 55–59, 1972.

[39] M. Sakano, N. Suetake, and E. Uchino, "Robust identification of motion blur parameters by using angles of gradient vectors," in *Proc. ISPACS*, 2006, pp. 522–525.

[40] A. Savakis and H. Trussell, "On the accuracy of PSF representation in image restoration," *IEEE Trans. Image Process.*, vol. 2, no. 2, pp. 252–259, Apr. 1993.

[41] Q. Shan, J. Jia, and A. Agarwala, "High-quality motion deblurring from a single image," *ACM Trans. Graph. SIGGRAPH*, vol. 27, no. 3, pp. 1–5, 2008.

[42] E. Stein and G. Weiss, *Introduction to Fourier Analysis on Euclidean Spaces*. Princeton, NJ, USA: Princeton University Press, 1971.

[43] T.-Y. Sun, S.-J. Ciou, C.-C. Liu, and C.-L. Huo, "Out-of-focus blur estimation for blind image deconvolution: Using particle swarm optimization," in *Proc. IEEE Int. Conf. SMC*, Oct. 2009, pp. 1627–1632.

[44] M. Tanaka, K. Yoneji, and M. Okutomi, "Motion blur parameter identification from a linearly blurred image," in *Proc. Int. Conf. ICCE*, 2007, pp. 1–2.

[45] A. Torralba and A. Oliva, "Statistics of natural image categories," *Netw. Comput. Neural Syst.*, vol. 14, no. 3, pp. 391–412, 2003.

[46] Y. Wang and W. Yin, "Compressed sensing via iterative support detection," Dept. Comput. Appl. Math., Rice Univ., Houston, TX, USA, Tech. Rep. TR09–30, 2009.

[47] L. Xu and J. Jia, "Two-phase kernel estimation for robust motion deblurring," in *Proc. 11th ECCV*, 2010, pp. 157–170.

[48] L. Xu, S. Zheng, and J. Jia, "Unnatural  $l_0$  sparse representations for natural image deblurring," in *Proc. IEEE Conf. CVPR*, Jan. 2013, pp. 2–4.

[49] L. Yuan, J. Sun, L. Quan, and H. Y. Shum, "Image deblurring with blurred/noisy image pairs," *ACM Trans. Graph. SIGGRAPH*, vol. 26, no. 3, pp. 1–5, 2007.



learning



## institution

**João P. Oliveira** received the E.E. and Ph.D. degrees in electrical and computer engineering from Instituto Superior Técnico, Engineering School, University of Lisbon, Portugal, in 2002 and 2010, respectively. He is currently a Researcher with the Pattern and Image Analysis Group, Instituto de Telecomunicações, Lisbon, Portugal. He is an Assistant Professor with the Department of Information Science and Technology, Instituto Universitário de Lisboa (ISCTE-IUL). His present research interests include signal and image processing, pattern recognition, and machine

**Mário A. T. Figueiredo** (S'87–M'95–SM'00–F'10) received the E.E., M.Sc., Ph.D., and Agregado degrees in electrical and computer electrical from Instituto Superior Técnico (IST), Engineering School, University of Lisbon (ULisbon), Portugal, in 1985, 1990, 1994, and 2004, respectively. He has been with the faculty of the Department of Electrical and Computer Engineering, IST, where he is currently a Professor. He is a group and area coordinator at Instituto de Telecomunicações, a private non-profit research

His research interests include signal processing and analysis, machine learning, and optimization. He is a fellow of the International Association for Pattern Recognition. From 2005 to 2010, he was a member of the Image, Video, and Multidimensional Signal Processing Technical Committee of the IEEE Signal Processing Society (SPS). He received the 2011 IEEE SPS Best Paper Award, the 1995 Portuguese IBM Scientific Prize, the 2008 UTL/Santander-Totta Scientific Prize. He has been an Associate Editor of several journals, namely the IEEE TRANSACTIONS ON IMAGE PROCESSING, the IEEE TRANSACTIONS ON PATTERN ANALYSIS AND MACHINE INTELLIGENCE, the IEEE TRANSACTIONS ON MOBILE COMPUTING, the *SIAM Journal on Imaging Science*, *Pattern Recognition Letters*, *Signal Processing*, and *Statistics and Computing*. He was a Co-Chair of the 2001 and 2003 Workshops on Energy Minimization Methods in Computer Vision and Pattern Recognition, a guest co-editor of special issues of several journals, and program/technical/organizing committee member of many international conferences.



**José M. Bioucas-Dias** (S'87–M'95) received the E.E., M.Sc., Ph.D., and Agregado degrees in electrical and computer engineering from Instituto Superior Técnico (IST), Engineering School, University of Lisbon (ULisbon), Portugal, in 1985, 1991, 1995, and 2007, respectively.

Since 1995, he has been with the Department of Electrical and Computer Engineering, IST, where he was an Assistant Professor from 1995 to 2007 and an Associate Professor since 2007. Since 1993, he has been a Senior Researcher with the Pattern and Image Analysis Group, Instituto de Telecomunicações, which is a private nonprofit research institution. His research interests include inverse problems, signal and image processing, pattern recognition, optimization, and remote sensing.

Dr. Bioucas-Dias was an Associate Editor for the IEEE TRANSACTIONS ON CIRCUITS AND SYSTEMS from 1997 to 2000 and is an Associate Editor for the IEEE TRANSACTIONS ON IMAGE PROCESSING and the IEEE TRANSACTIONS ON GEOSCIENCE AND REMOTE SENSING. He was a Guest Editor of the Special Issue on Spectral Unmixing of Remotely Sensed Data of the IEEE TRANSACTIONS ON GEOSCIENCE AND REMOTE SENSING, of the Special Issue on Hyperspectral Image and Signal Processing of the IEEE JOURNAL OF SELECTED TOPICS IN APPLIED EARTH OBSERVATIONS AND REMOTE SENSING, and is a Guest Editor of the Special Issue on Signal and Image Processing in Hyperspectral Remote Sensing of the IEEE SIGNAL PROCESSING MAGAZINE. He was the General Co-Chair of the 3rd IEEE GRSS Workshop on Hyperspectral Image and Signal Processing, Evolution in Remote sensing (WHISPERS'2011), and has been a member of program/technical committees of several international conferences.